

Vortex Induction via Anisotropy Stabilized Light-Matter Interaction

R. Barboza,^{1,2} U. Bortolozzo,¹ G. Assanto,² E. Vidal-Henriquez,³ M. G. Clerc,³ and S. Residori¹

¹*INLN, Université de Nice-Sophia Antipolis, CNRS, 1361 Route des Lucioles, 06560 Valbonne, France*

²*NooEL-Nonlinear Optics and OptoElectronics Lab, University Roma Tre, Via della Vasca Navale 84, 00146 Rome, Italy*

³*Departamento de Física, FCFM, Universidad de Chile, Casilla 487-3, Santiago, Chile*

(Received 3 July 2012; published 1 October 2012)

By sending circularly polarized light beams onto a homeotropic nematic liquid crystal cell with a photosensitive wall, we are able to locally induce spontaneous matter vortices that remain, each, stable and trapped at the chosen location. We discuss the dual light-matter nature of the created vortices and demonstrate the ability of the system to create optical vortices with opposite topological charges that, consistent with angular momentum conservation, both derive from the same defect created in the liquid crystal texture. Theoretically, we identify a self-stabilizing mechanism for the matter vortex, which is provided by the concurrency of light-induced gradients and anisotropy of the elastic constants that characterize the deformation of the liquid crystal medium.

DOI: [10.1103/PhysRevLett.109.143901](https://doi.org/10.1103/PhysRevLett.109.143901)

PACS numbers: 42.25.-p, 42.50.Tx, 42.70.Df, 42.70.Gi

Optical vortices [1–3] are receiving considerable attention in view of their potential applications. We can mention, for instance, the exchange of angular momentum between light and matter [4], the realization of optical tweezers [5–7], the implementation of quantum computational schemes [8], the improvement of astronomical imaging [9], and wave front sensors [10]. Among the different methods envisaged to produce optical vortices, Marrucci *et al.* realized *ad hoc* matter defects with pre-imposed director orientation in liquid crystal (LC) samples, the so-called *q*-plates, and demonstrated that they can efficiently perform the transfer from spin-to-orbital angular momentum for circularly polarized beams [11]. This approach exploits the anisotropic nature of LC media. However, besides anisotropy, which is at the basis of their large electro-optic response, LCs are also characterized by their self-reconfiguring capability, either under the action of light [12] or of electric fields [13]. In this framework, optical vortices are expected to derive directly from the appearance of defects in the LC texture, for instance, under the application of an electric field, as it was shown for dislocations in cholesteric LCs [14] and, more recently, for umbilics in homeotropic nematics [15,16]. In particular, the umbilic defect naturally possesses a vortex-like morphology, making it attractive for realizing the matter template able to impress a helical structure on an incoming wave front. Nonetheless, major problems arise when practical implementations are aimed at, because soft-matter defects are dissipative structures that obey a complex Ginzburg-Landau equation (CGLE) and undergo a coarsening dynamics ruled by their mutual interaction and annihilation [17]. Therefore, they are unstable (see, e.g., Refs. [2,13]), usually limited to a single defect pair per sample or a defect-free sample, and without the possibility of controlled addressing.

In this Letter, we propose a novel approach for robust vortex induction, which relies on the association of nematic LCs with a photosensitive substrate, to realize a homeotropic light-valve geometry. By transforming the intensity of the incoming light into a voltage that locally applies only across the illuminated regions, the LC light valve (LCLV) enables the local induction of stable and positionally reconfigurable matter vortices, trapped at each chosen location. These matter vortices, in turn, give rise to optical vortices via the transfer of spin-to-orbital angular momentum onto the incoming light. We demonstrate the ability to control optical vortices of opposite topological charges that, consistent with angular momentum conservation, both derive from the same matter defect created in the LC layer. Then, we show the possibility of inducing adjacent independent vortices, with input beams separated by a transverse distance of the same order of their size. Our experimental results are supported by a theoretical explanation of matter vortex stability, which, on the basis of a modified Ginzburg-Landau model with anisotropic terms [18], identifies a self-stabilizing and self-centering mechanism. The latter derives from the concurrency of light-induced gradients and anisotropy of the elastic constants that describe the deformation of the LC medium. As a result, equilibrium vortex positions are found near the center of the illuminated region. Note that, compared to other techniques, our method to create optical vortices has several advantages, such as self-induction, reconfigurability, and self-centering properties, together with the low power of the beams that induce the vortices.

Experimental setup.— The setup for vortex induction is sketched in Fig. 1(a). The LCLV is prepared by interposing a $d = 15 \mu\text{m}$ layer of nematic LC (MLC 6608 from Merck) in between two parallel interfaces, a glass plate and a slab of the transparent photoconductor $\text{Bi}_{12}\text{SiO}_{20}$ (BSO), $25 \times 25 \text{ mm}^2$, thickness 1 mm. The interior surfaces are

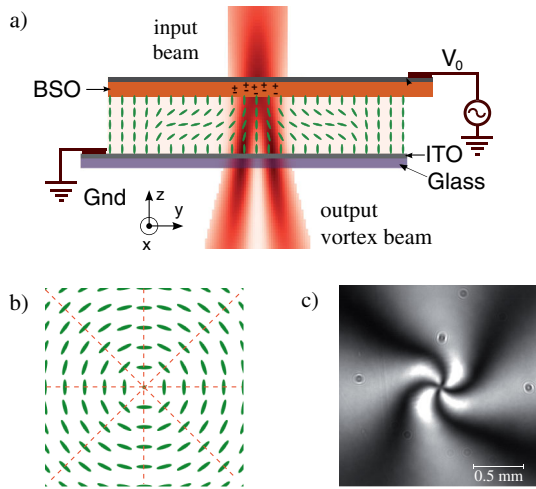


FIG. 1 (color online). (a) Schematic setup for vortex induction: a circularly polarized beam is incident on the photoconductive side of the LCLV; the voltage V_0 is such that only the illuminated region undergoes the Fréedericksz transition; when reorienting, the LC molecules follow the circular pattern associated with the electric field and create a matter vortex; this, in turn, induces an optical vortex at the exit. Matter vortex: (b) schematic sketch of the molecular director in the x - y plane; the dashed lines represent the transverse lines of the electric field; (c) intensity profile measured under white light illumination, crossed polarizers.

treated to obtain the homeotropic anchoring of the LC, that is, with the nematic director orthogonal to the confining walls. The outer surface of the photoconductor and inner surface of the glass plate are uniformly coated with thin indium-tin-oxide transparent electrodes for applying a voltage V_0 across the cell. The employed LC has a negative dielectric anisotropy, $\epsilon_a = \epsilon_{\parallel} - \epsilon_{\perp} < 0$, with ϵ_{\parallel} and ϵ_{\perp} the dielectric susceptibility for the electric fields parallel and orthogonal, respectively, to the molecular director.

When a bias V_0 is applied to the LCLV beyond the Fréedericksz transition voltage of the cell V_{FT} , the molecules tend to reorient perpendicularly to the (low frequency) electric field because of the negative ϵ_a ; hence, since $\vec{E} = V_s/d\hat{z}$ (with V_s the voltage at the LC-BSO interface) is applied along the longitudinal z direction and the 2π azimuthal degeneracy imposes rotational invariance around it, the LC molecules can arbitrarily align in any direction, spontaneously forming spatial domains separated by walls, loops, and umbilic defects or vortices [13]. In the present experiment, we keep $V_0 \lesssim V_{FT}$ in order to avoid the spontaneous reorientation while bringing the molecules close to the transition point. When a light beam is incident onto the photosensitive wall of the LCLV, due to the photo-generated charges, there is a slight increase of the voltage, which effectively drops across the LC region underneath: the Fréedericksz threshold is locally overcome and the molecules start reorienting, following the intensity gradients associated with the Gaussian beam profile. Moreover, if the input beam is circularly polarized, the

reorienting molecules follow the rotational structure of the associated electric-field lines. Hence, a vortex-like defect is spontaneously induced in the matter texture. A schematic sketch of the molecular director in the x - y plane is shown in Fig. 1(b), while Fig. 1(c) reports an experimental vortex profile observed under white light illumination and crossed polarizers.

Vortex induction.—To prove the vortex induction, a laser beam of wavelength $\lambda = 632$ nm and power $P = 0.55$ mW is focused on a diameter of $395 \mu\text{m}$ onto the photoconductive side of the LCLV. The input beam polarization is taken to be either right-handed (RH) or left-handed (LH) circular. Typical snapshots of the output beams observed in the two cases are shown in Fig. 2 for $V_0 = 24$ V rms at a frequency of 100 Hz. The intensity profiles, Figs. 2(a) and 2(b), show that the two beams are Gauss-Laguerre—like modes with complex amplitude of the form $\Phi(x, y, z) = \psi(r, z) \exp(ikz + m\theta)$, with ψ , k , and m representing, respectively, the amplitude, the wave vector, and the topological charge. Here, (r, θ, z) are the cylindrical coordinates associated to (x, y, z) . The output beam polarization for a LH (RH) circular input beam has been verified to be RH (LH) circular. The topological charge can be estimated from the interference patterns displayed in Figs. 2(c)–2(f), for spherical and respectively planar wave front of the reference beam. The two-arm spirals in the first case and the two dislocations in the fringe patterns in the second case are robust and

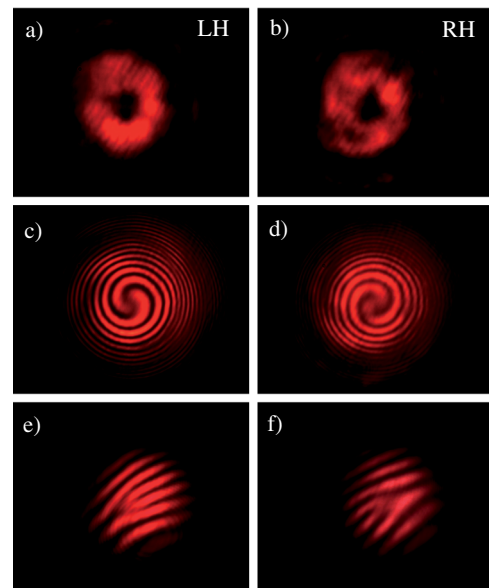


FIG. 2 (color online). Experimental observation of optical vortices induced by left-handed, LH (right-handed, RH), circularly polarized input beams: (a, b) output intensity showing Gauss-Laguerre beams, (c, d) fringe patterns after interference with a curved wave front, (e, f) patterns after interference with a planar wave front; (c, e) $m = +2$, (d, f) $m = -2$; $V_0 = 24 V_{pp}$, $P = 0.55$ mW.

reproducible. The topological charge transferred to the output beam is $m = +2$ ($m = -2$) for the LH (RH) circularly polarized input beam. Correspondingly, the spin-to-orbital angular momentum conversion is consistent with a q plate with charge $q = +1$ [11] and the matter vortex is an umbilic-like defect with winding number $+1$. Note that due to the nature of the matter vortex, $m = \pm 2$ are the only possible values for the transferred topological charge.

The efficiency of the spin-to-orbital angular momentum transfer is quantified by recording the power of the output Gauss-Laguerre mode P_{GL02} when varying the voltage V_{pp} applied to the LCLV and for various input powers. The measurements are carried out by placing a $\lambda/4$ wave plate on the path of the output beam, projecting the circularly converted RH (LH) for LH (RH) input, and the residual polarization components into two orthogonal linear polarizations, and measuring the intensity of the one carrying the topological charge [11]. The results are plotted in Fig. 3, where the value of the input power is marked along each curve. The threshold voltage V_{FT} slightly depends on the input power. The peak of the response curves corresponds to a π overall phase retardation between the ordinary and extraordinary components in the LC layer. Finally, by launching two adjacent input beams, we verify that two stable and independent vortices are obtained. Figure 4 shows the vortices induced for two RH [Fig. 4(a)], two LH [Fig. 4(b)], and LH and RH [Fig. 4(c)] input beams, respectively. The minimal separation at which the two vortices can be induced coincides approximately with the size of the individual input spots.

Mechanism for self-stabilization of the matter vortex.— To describe the mechanism of the creation and pinning of matter vortices, we derive a model in the vicinity of the Fréedericksz transition, a limit where analytical results are accessible, as nematic LC molecules are weakly tilted from

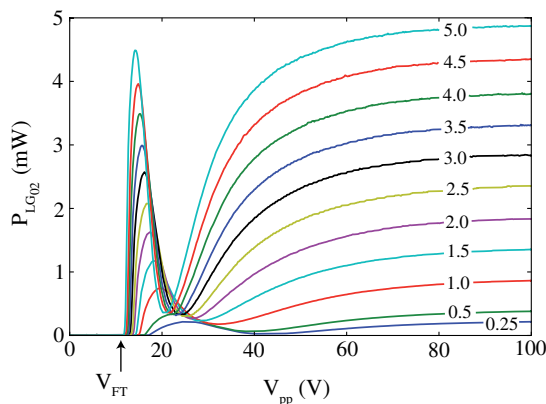


FIG. 3 (color online). Efficiency of spin-to-orbital angular momentum transfer versus experimental parameters. The power of the output Gauss-Laguerre mode P_{GL02} is plotted as a function of the voltage V_{pp} applied to the light valve and for various input powers as marked (in mW) on each curve; V_{FT} is the Fréedericksz transition voltage.

the longitudinal axis \hat{z} and backflow effects can be neglected. The dynamical equation for the molecular director \vec{n} reads [13] $\gamma \partial_t \vec{n} = K_3 [\nabla^2 \vec{n} - \vec{n}(\vec{n} \cdot \nabla^2 \vec{n})] + (K_3 - K_1)[\vec{n}(\vec{n} \cdot \vec{\nabla})(\vec{\nabla} \cdot \vec{n}) - \vec{\nabla}(\vec{n} \cdot \vec{\nabla})] + 2(K_2 - K_3) \times [(\vec{n} \cdot \vec{\nabla} \times \vec{n})(\vec{n}(\vec{n} \cdot \vec{\nabla} \times \vec{n}) - \vec{\nabla} \times \vec{n}) + \vec{n} \times \vec{\nabla}(\vec{n} \cdot \vec{\nabla} \times \vec{n})] + \epsilon_a(\vec{n} \cdot \vec{E})[\vec{E} - \vec{n}(\vec{n} \cdot \vec{E})]$, where γ is the LC rotational viscosity, and $\{K_1, K_2, K_3\}$ are the NLC elastic constants. Under uniform illumination, $\vec{E} = V/d\hat{z} \equiv E_z\hat{z}$, and the homeotropic state $\vec{n} = \hat{z}$ undergoes a stationary instability for critical values of the voltage, which match the Fréedericksz threshold $V_{FT} = \sqrt{-K_3\pi^2/\epsilon_a}$. Close to the transition point, we introduce the ansatz

$$\vec{n} \approx \begin{pmatrix} u(\vec{r}, t) \sin\left(\frac{\pi z}{d}\right) \\ v(\vec{r}, t) \sin\left(\frac{\pi z}{d}\right) \\ 1 - \frac{(u^2 + v^2)}{2} \sin^2\left(\frac{\pi z}{d}\right) \end{pmatrix},$$

with $\vec{r} = (x, y)$ the transverse coordinates. By using the complex field $A(\vec{\rho}, t) = (u + iv)/\sqrt{4d^2\gamma/\pi^2(2K_1 - 3K_3)}$ and scaling the space as $\vec{\rho} = \vec{r}\sqrt{2/(K_1 + K_2)}$, after straightforward calculations we obtain the anisotropic CGLE [18]

$$\partial_t A = \mu_0 A - |A|^2 A + \nabla_{\perp}^2 A + \delta \partial_{\eta} \eta \bar{A}, \quad (1)$$

where $\mu_0 \equiv (-\epsilon_a E_z^2 - K_3 \pi^2/d^2)/\gamma$ is the bifurcation parameter, $\delta \equiv (K_1 - K_2)/(K_1 + K_2)$ accounts for the elastic anisotropy, $\partial_{\eta} = \partial_x + i\partial_y$, and $\nabla_{\perp}^2 \equiv \partial_{xx} + \partial_{yy} = \partial_{\eta} \partial_{\bar{\eta}}$. When neglecting anisotropy, $\delta = 0$, the above model reduces to the CGLE with real coefficients, which admits stable dissipative vortex solutions with topological charge (winding number) ± 1 [2]. The presence of anisotropy breaks the symmetry, and the $+1$ vortex is energetically favored with respect to -1 . Anisotropy, therefore, strongly influences the system response.

When the illumination has a Gaussian profile, in order to calculate the nonuniform voltage V across the LC layer, we have to consider the Laplace equation

$$\nabla^2 V + \frac{\epsilon_a}{\epsilon_{\perp}} \partial_z^2 V = 0, \quad (2)$$

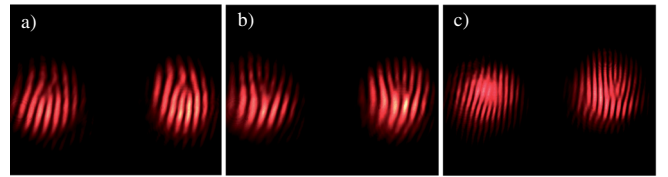


FIG. 4 (color online). Observed adjacent vortex beams for (a) right-handed (RH), (b) left-handed (LH), (c) one RH and one LH input beams; $V_0 = 24 V_{pp}$, $P = 0.55$ mW.

where we neglect the effect of director reorientation. By taking the boundary conditions $V(x, y, 0) = 0$ and $V(x, y, d) = V_s(x, y)$, with V_s the voltage distribution at the surface, we can find a solution of the form

$$V(x, y, z) = \int \frac{\sinh(\alpha qz)}{\sinh(\alpha qd)} V_s(\vec{q}) e^{i\vec{q}\cdot\vec{r}} d\vec{q}^2, \quad (3)$$

with $\alpha = \sqrt{1 + \epsilon_a/\epsilon_\perp}$. In the limit of slow gradient, we can approximate $\sinh(\alpha qd) \sim \alpha qd$ and, therefore, take $V(x, y, z) = V_s(x, y)z/d$; that is, we can separate the transverse contribution of the electric field from its vertical one. We can, then, calculate the pinning force of a radially symmetric potential on a stationary vortex. The total energy of the system can be written as $W = W_D + W_{\text{INT}}$, with $W_D = \frac{1}{2} \int K_1 (\nabla^2 \cdot \vec{n}) + K_2 (\vec{n} \cdot \nabla \times \vec{n}) + K_3 (\nabla \times \vec{n})^2$ and $W_{\text{INT}} = -\frac{1}{2} \epsilon_a \int (\vec{n} \cdot \nabla V)^2$ the deformation and the interaction energy, respectively. By taking as an ansatz for $V_s(x, y)$ a Gaussian profile of width w and amplitude V_1 , that is, $V_s(\vec{r}) = V_{s_0} + V_1 \exp(-2r^2/w^2)$, and by inserting it into the expression for W_{INT} , after straightforward calculations, we find $W_{\text{INT}} = -\frac{\pi}{4} \epsilon_a d V_1^2 [\cos(2\chi) \times \exp(-4L^2/w^2) + 1]$, where L is the distance of the vortex core from the center of the radially symmetric potential and χ is the angle of the nematic director in the transverse plane with respect to the radial lines of the electric field. Since in our case, $\epsilon_a < 0$, the defect has a minimum energy when $\chi = \pi/2$ [19]; that is, the director is orthogonal to the field lines [see Fig. 1(b)]. By accounting for this transverse correction, the bifurcation parameter is modified as follows:

$$\mu(\rho) = \mu_o + \epsilon_a d^2 (1/3 - 1/2\pi^2) |\partial_\eta E_z|^2 / \gamma \equiv \mu_o + \mu_1, \quad (4)$$

which incorporates light-induced gradients, with μ_o the same as before and $E_z = V_s(\vec{r})/d$. A circular region is below or above the Fréedericksz transition threshold when $\mu_o + \mu_1 < 0$ or $\mu_o + \mu_1 > 0$, respectively. Moreover, first-order corrections introduce in Eq. (1) transverse pinning and forcing terms that have the form of $(1/3 - 1/\pi^2)(\partial_\eta E_z)^2 \bar{A} + 2L/\pi E_z \partial_\eta E_z$ [20].

We perform numerical simulations of the modified Eq. (1), starting from an initial homeotropic condition $A = 0$ in the presence of noise and for $\mu_o + \mu_1 > 0$. At the beginning, we observe the creation of a large number of vortices, later accompanied by a coarsening evolution through the annihilation of oppositely charged vortices, after which a few vortices survive. In the isotropic case, $\delta = 0$ and no transverse pinning terms, we observe that the vortices move away from the center, then they disappear by exiting through the edges, and finally there would be no vortex left in the system. However, when we consider the joint effects of transverse pinning and anisotropy, $\delta \neq 0$, the scenario changes. While the negatively charged vortices continue to move towards the perimeter of the circle,

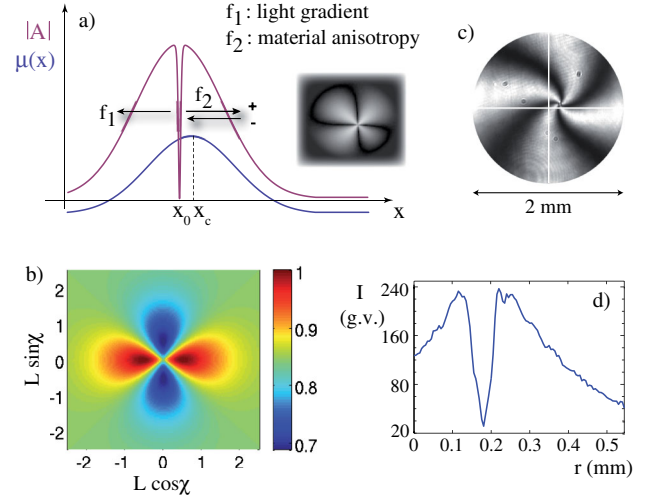


FIG. 5 (color online). Effect of the anisotropy on vortex stabilization. (a) Calculated vortex profile; f_1 and f_2 are the forces generated by the parameter gradients and anisotropy, respectively; a numerically simulated vortex is shown in the inset. (b) Pinning potential showing the equilibrium vortex positions near the center; χ is the angle of the nematic director in the transverse plane. (c) Photograph of a stable experimental vortex; the cross indicates the center of the illuminated region. (d) Corresponding intensity profile versus the radial coordinate r ; g.v. stands for gray values on the camera.

where they finally vanish, the vortices with positive charges repel each other and also disappear at the edges, but one of them remains pinned at an equilibrium position close to the center, with a small but finite offset.

Figure 5 illustrates the role of anisotropy on vortex stabilization. The equilibrium position can be interpreted as resulting from the balance of two forces: a radial force induced by the parameter gradients, which tend to push the vortices to the edges of the illuminated region, and a force induced by the anisotropic deformation, which is opposite to the light gradients. In Fig. 5(a), the numerically calculated vortex profile is plotted together with parameter variation, with the arrows indicating the forces caused by light gradients and anisotropy respectively. The direction of the force due to anisotropy depends on the vortex charge. Because of the balance between the two opposite forces, the vortex core is at an equilibrium position x_0 close to but not exactly coincident with the center x_c of the illuminated region. Figure 5(b) shows the numerically calculated potential, in which four equilibrium vortex positions near the center are visible. An experimental example of a stable experimental vortex is shown in Fig. 5(c). The corresponding intensity profile is plotted in Fig. 5(d) against the radial coordinate r .

Conclusions.—By using a nematic LC in a homeotropic LV geometry, we experimentally demonstrated a novel robust phenomenon of controlled vortex induction, which is, at the same time, low power, self-induced, self-stabilizing, and positionally stable. We have highlighted

the relative role of the matter vortex and optical vortex. The latter is mediated by the spin-to-orbital angular momentum transfer of photons. Besides, we have pinpointed the theoretical basis of the vortex stability by means of a generalized Ginzburg-Landau model that takes into account medium anisotropy.

M. G. C., U. B., and S. R. acknowledge financial support from the ANR international program Project No. ANR-2010-INTB-402-02 (ANR-CONICYT39), “COLORS.” M. G. C. acknowledges funding from the FONDECYT Project No. 1120320 and Anillo Grant No. ACT127. G. A. acknowledges travel funding from the Program for Internationalisation at University Roma Tre.

-
- [1] J. F. Nye and M. V. Berry, *Proc. R. Soc. A* **336**, 165 (1974).
 - [2] L. M. Pismen, *Vortices in Nonlinear Fields* (Oxford Science Publications, New York, 1999).
 - [3] M. S. Soskin and M. V. Vasnetov, *Prog. Opt.* **42**, 219 (2001).
 - [4] L. Allen, M. W. Beijersbergen, R. J. C. Spreeuw, and J. P. Woerdman, *Phys. Rev. A* **45**, 8185 (1992).
 - [5] N. B. Simpson, L. Allen, and M. J. Padgett, *J. Mod. Opt.* **43**, 2485 (1996).
 - [6] J. E. Curtis, B. A. Koss, and D. G. Grier, *Opt. Commun.* **207**, 169 (2002).
 - [7] D. G. Grier, *Nature (London)* **424**, 810 (2003).
 - [8] H. H. Arnaut and G. A. Barbosa, *Phys. Rev. Lett.* **85**, 286 (2000).
 - [9] F. Tamburini, G. Anzolin, G. Umbrico, A. Bianchini, and C. Barbieri, *Phys. Rev. Lett.* **97**, 163903 (2006).
 - [10] K. Murphy and C. Dainty, *Opt. Express* **20**, 4988 (2012).
 - [11] L. Marrucci, C. Manzo, and D. Paparo, *Phys. Rev. Lett.* **96**, 163905 (2006).
 - [12] I. C. Khoo, *Optics and Nonlinear Optics of Liquid Crystals* (World Scientific, Singapore, 1993).
 - [13] P. G. de Gennes and J. Prost, *The Physics of Liquid Crystals* (Oxford Science Publications, New York, 1993), 2nd. ed.
 - [14] D. Voloschenko and O. D. Lavrentovich, *Opt. Lett.* **25**, 317 (2000).
 - [15] E. Brasselet and C. Loussert, *Opt. Lett.* **36**, 719 (2011).
 - [16] E. Brasselet, *Phys. Rev. Lett.* **108**, 087801 (2012).
 - [17] I. Dierking, O. Marshall, J. Wright, and N. Bulleid, *Phys. Rev. E* **71**, 061709 (2005).
 - [18] T. Frisch, S. Rica, P. Couillet, and J. M. Gilli, *Phys. Rev. Lett.* **72**, 1471 (1994).
 - [19] S. Chandrasekhar, *Liquid Crystals* (Cambridge University, New York, 1977).
 - [20] The full model derivation will be reported elsewhere.